Numerical Design of a Reactor-Heat Exchanger Combined Unit for Ammonia-$SrCl_2$ Thermochemical Storage System

Saman N. Gunasekara[1], Stefano Soprani[2], Anastasiia Karabanova[2], Viktoria Martin[1] and Didier Blanchard [2]

[1] Department of Energy Technology, KTH Royal Institute of Technology, Stockholm (Sweden).

[2] Department of Energy Conversion and Storage, Technical University of Denmark (DTU), Roskilde (Denmark).

Abstract

This work presents the design of a reactor-heat exchanger combined unit using COMSOL transient simulations in 2D for a thermochemical storage (TCS) system of NH_3-$SrCl_2$ (absorption-desorption of $SrCl_2{\cdot}NH_3$ and $SrCl_2{\cdot}8NH_3$). TCS with NH_3-metal halide reactions is emerging, with many packed-bed reactors often incorporating salt with expanded graphite (EG) to improve thermal conductivity. Similarly, a packed-bed reactor is chosen here using $SrCl_2$-EG composite, for a reaction pressure of 8 bar, accommodating desorption above 82 °C and absorption below 79 °C. The aim here is to find a simple and cost-effective reactor-heat exchanger (HEX) combined unit to store 0.5 kWh heat (1.1 kg of $SrCl_2{\cdot}NH_3$ forming 1.8 kg of $SrCl_2{\cdot}8NH_3$). From several HEX configurations, the first configuration is modelled here. This is contains three reaction media cylinders (a composite of 87.5% w/w of $SrCl_2{\cdot}8NH_3$ in EG) sandwiching two units of tube-in-tube (TinT) HEXs. A stationary study for the heat transfer fluid (HTF) velocity analysis is coupled with a time-dependent study for the reaction phenomena, respectively for the salt-alone and salt-EG composite. For 15 hours reaction time, the reaction advancement (above 0.85) was enhanced significantly in the salt-EG composite, which was only above 0.55 for the salt-only case. The reaction progression is the slowest in the bottom of the innermost reaction media, where the HTF temperature is the lowest. Thus, an additional HEX unit along the center-axis of the reactor appears suitable to reduce the reaction time. As next, the effect of HEX thickness, number of TinT units, as well as other reactor-HEX configurations will be analyzed to choose the optimal setup.

Keywords: Ammonia-$SrCl_2$, absorption, desorption, thermochemical heat storage (TCS), reactor, COMSOL

1 Introduction

Thermal energy storage (TES) is a key technology in enabling more efficient and effective management of energy systems, by facilitating peak shaving and load shifting (Barzin, Chen, Young, & Farid, 2015), harvesting waste thermal energy (Chiu et al. 2016, Fujii et al. 2019), and renewable energy sources integration, particularly with solar energy (Frazzica and Freni 2017, Valverde et al. 2017). Thermochemical storage (TCS) systems storing the heats of reversible chemical reactions are an attractive type of TES, with, very high storage densities that offer temperature-flexible design. TCS systems are mainly two-fold based on the operating mechanism: using adsorption, or absorption. Among the absorption-based TCS systems involving non-water reaction pairs, many employ the reaction between NH_3 and a metal halide such as $SrCl_2$, $MnCl_2$, $CaCl_2$, $BaCl_2$, $MgCl_2$, and NH_4Cl_2 (Erhard, Spindler, and Hahne 1998, Li et al. 2009, Bao et al. 2012, NagaMalleswara Rao, Ram Gopal, and Bhattacharyya 2013, Li, Wang, and Yan 2015, Kuwata et al. 2016, Soprani 2016, Li et al. 2016, Jiang et al. 2016, Mofidi and Udell 2017, Al-Zareer, Dincer, and Rosen 2017). As the thermal conductivity of these salts are considerably low, to improve heat transfer and thus reaction kinetics inside the reactors, incorporating the metal halide into e.g. expanded graphite (EG) matrices have also been analyzed (Bao et al. 2012, Li et al. 2009, Li et al. 2010, Jiang et al. 2016, Mofidi and Udell 2017). The evaluated reactor configurations include e.g. simple packed-beds with an axial flow of NH_3 in (NagaMalleswara Rao et al., 2013), (Li et al., 2016), a packed-bed using stainless-steel (SS) honeycomb disks containing salt with NH_3 flow through the disks (Soprani, 2016), a permeable piston-controlled packed-bed (Mofidi & Udell, 2017), among others. These heat exchanger (HEX) configurations so far are of simple construction, e.g.: an HTF bath where the reaction media pipes are immersed (Erhard, Spindler, and Hahne 1998); an annular jacket coupled with a center-line HEX (Bao et al. 2012, NagaMalleswara Rao, Ram Gopal, and Bhattacharyya 2013); a double-pipe HEX (Li, Wang, and Yan 2015, Li et al. 2016); an HTF bath adjacent to a packed bed of reactants (Kuwata et al. 2016); a W-tube HEX (Soprani 2016); as an annular HEX (Jiang et al. 2016) or a heating rod (Mofidi and Udell 2017) along the center-axis of packed bed.

doi:10.18086/swc.2019.24.03 Available at http://proceedings.ises.org

With this background, the aim of this study is to present new knowledge on the combined reactor-HEXs configurations that significantly improve the heat transfer properties and reaction kinetics of NH_3-metal halide TCS systems. Specifically, out of several new HEX configurations in combine with an EG matrix for better heat transfer will be explored through numerical simulations, with reaction advancement (a), as well as temperature and ammonia velocity evolution within the reactor as performance criteria. This is expected to achieved through transient 2D simulations with COMSOL Multiphysics (COMSOL Inc., 2019), for the NH_3-$SrCl_2$ system involving the absorption/desorption between $SrCl_2{\cdot}NH_3$ and $SrCl_2{\cdot}8NH_3$. With these COMSOL numerical simulations, it is here expected to determine the optimal reactor-heat exchanger configuration for improved reaction kinetics in the system, starting with the presented configuration and comparisons to be made with some other configurations in continuation.

2 Methodology

The considered chemical reaction of the system NH_3-$SrCl_2$ is detailed in (eq. 1). This reaction has a reaction enthalpy (ΔH) and entropy (ΔS) of 41.4 kJ mol_{NH3}^{-1} and 230 J mol^{-1} K^{-1} (Lysgaard et al., 2012) respectively. For the targeted heat storage capacity of 0.5 kWh (i.e., 1800 kJ), the stoichiometric amount of NH_3 needed is 43.48 mol, to react with 6.21 mol (i.e., 1.09 kg) of $SrCl_2{\cdot}NH_{3(s)}$ to produce 6.21 mol (i.e., 1.83 kg) of $SrCl_2{\cdot}8NH_{3(s)}$. The equilibrium conditions are chosen according to the Van't Hoff's equation (Soprani 2016, Lysgaard et al. 2012), at 8 bar pressure, with absorption at 79 ℃ and desorption at 82 ℃.

$$7\ NH_{3(g)} + SrCl_2{\cdot}NH_{3\ (s)} \leftrightarrows SrCl_2{\cdot}8NH_{3\ (s)} + \Delta H \qquad \text{(eq. 1)}$$

1.1. Reactor sizing

To realize aim of finding an optimal reactor-HEX configuration, several specific configurations are chosen, with better HEX-configurations, e.g. as compared to state-of-the-art as summarized in section 1. From these chosen alternatives, as the first step, a cylindrical packed-bed reactor (vessel in SS 316) is considered herein. This is embedding $SrCl_2{\cdot}8NH_3$-EG composite in three respective cylindrical blocks sandwiched between two annular tube-in-tube (TinT) heat exchangers in Al, as shown in Figure 1. These dimensions along the indicated parameters are explained and summarized in Table 1, which were calculated using the following data. The simplicity for cost-effective manufacturing of this combined unit has been a priority in choosing this particular reactor-HEXs configuration here. Thus, e.g. the reactor vessel diameter and thickness were chosen within existing commercial stainless steel pipe dimensions from (Damstahl, 1998) suitable for the system pressures (allowing a safety margin as well). The employed expanded graphite (EG) boards are from (SGL CARBON GmbH, 2019).

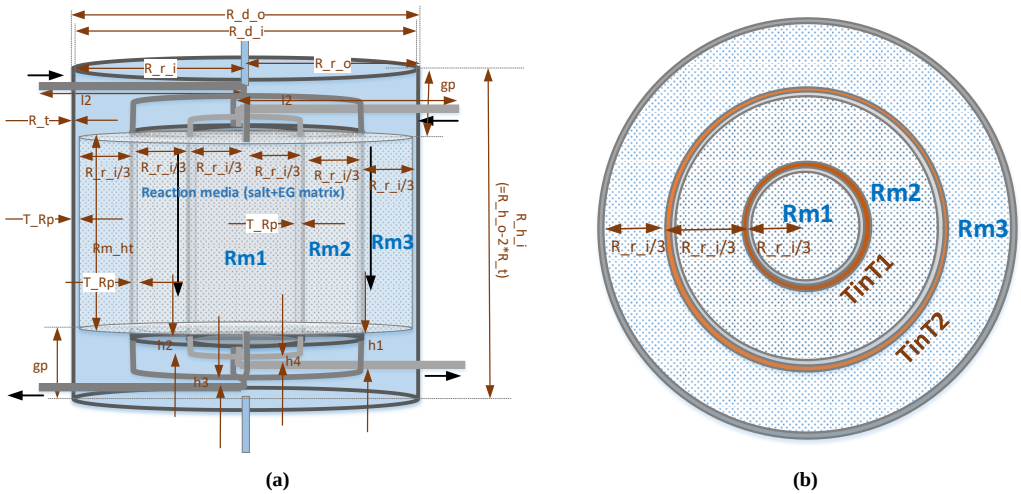

Figure 1. The chosen reactor-Heat Exchanger configuration and dimensions (Rm: reaction media, TinT: tube-in-tube HEX)

The required amount of reaction media (Rm), i.e., the salt-EG board composite, was calculated based on own experimental data (conducted at DTU) for salt compression tests into Sigratherm (SGL) EG boards L 20/1500 (SGL CARBON GmbH, 2019). The tests indicated that this $SrCl_2$-EG composite (bulk density of 820 kg m^{-3}) can be made successfully to contain 79% w/w $SrCl_2$ (molar mass: 158.52 g mol^{-1}). After ammoniation tests, the density of this composite became 1380 kg m^{-3}, thus accounting for 87.5% w/w of $SrCl_2.8NH_3$. With a bulk density of 1000 kg m^{-3} of $SrCl_2.8NH_3$ (Soprani 2016, Lysgaard et al. 2012), the required EG board volume of L 20/1500 type is thus found to be 0.00152 m^3 (for 0.5 kWh energy storage capacity). To accommodate any compacting inhomogeneity, it was

decided to use 30% more volume of the board, thus accounting for 0.00198 m^3 (~2 l). As during the experiments, neither the salt compacting nor ammoniation expanded the volume of the EG board from the original size, this volume corresponds to the total volume of the reaction media, i.e., the salt-EG composite. There, the reaction media height was chosen iteratively to achieve a reaction media volume to match this 130% of the EG volume. This chosen height results in real reaction media volume of 0.00210 m^3, which is therefore sufficient (as it is greater than 0.00198 m^3). The volume fraction of $SrCl_2{\cdot}8NH_3$ and EG in this media is 0.952 and 0.0476 (excluding pore volume), respectively.

Table 1. The chosen reactor-heat exchanger dimensions

Parameter	Value	Unit	Description
R_r_o	84.15	mm	Reactor external radius (Damstahl, 1998). R_d_o=2·R_r_o
R_t	2.6	mm	Reactor wall thickness (Damstahl, 1998).
R_r_i	81.55	mm	Reactor internal radius (Damstahl, 1998). R_d_i=2·R_r_i
HEX_d_i	4	mm	Heat exchanger tubing internal diameter (Swagelok, 2019)
HEX_d_o	6	mm	Heat exchanger tubing external diameter (Swagelok, 2019)
l2	94.15	mm	Length of the HEX tube inlet and outlet horizontal pieces, assumed,
T_Rp	0	mm	The gaps between each reactor component (e.g. reaction media and TinT walls), assumed negligible.
TinT1_r	27.18	mm	Tube-in-in-tube 1 (inner) HEX radius, to the center of the HEX annulus
TinT2_r	54.37	mm	Tube-in-in-tube 2 (outer) HEX radius, to the center of the HEX annulus
TinT_tb_t	2.6	mm	Wall thickness of each TinT cylindrical tube, assumed = R_t
HEX_t	5	mm	The effective HEX thickness (for heat transfer fluid flow) of each TinT
TinT1_ro	37.38	mm	The outer radius (including HEX walls and HEX_t) of TinT1 cylinder
TinT1_ri	27.2	mm	The inner radius (excluding HEX walls and HEX_t) of TinT1 cylinder
TinT2_ro	64.57	mm	The outer radius (including HEX walls and HEX_t) of TinT2 cylinder
TinT2_ri	54.4	mm	The inner radius (excluding HEX walls and HEX_t) of TinT2 cylinder
Rm1_r	27.2	mm	The radius of the inner reaction media cylinder
Rm2_r	54.4	mm	The outer radius of the middle reaction media cylinder
Rm3_r	81.6	mm	The outer radius of the outer reaction media cylinder
Rm_v_1.3	0.00198	m3	Total volume of reaction media required for 1.3% EG volume (1.98 l)
Rm_ht	140.0	mm	Reaction media height, iteratively calculated to obtain the required reaction media volume
HEX_h	140.0	mm	Assumed as the same as Rm_ht
Rm1_v	0.000325	m^3	The volume of inner reaction media cylinder
Rm2_v	0.000685	m^3	The volume of middle reaction media cylinder
Rm3_v	0.001091	m^3	The volume of outer reaction media cylinder
Rm_v_calc	0.002102	m^3	The total real volume of the reaction media (=Rm1_v+ Rm2_v+ Rm3_v)
h1	105.0	mm	Heights of the vertical parts of the HEX inlet and outlets to/from TinT2
h2	35.0	mm	Heights of the vertical parts of the HEX inlet and outlets to/from TinT1
h3, h4	25.0	mm	Heights of the vertical HEX inlet/outlet connectors to/from TinT1 and TinT2
gp	80	mm	Empty reaction vessel spaces above and below reaction media, assumed
R_hi	305.2	mm	Total reactor height, inner
R_ho	310.4	mm	Total reactor height, outer
R_Vt	0.006905	m^3	Total reactor volume (6.91 l)

1.2. Reactor-heat exchanger numerical simulation using COMSOL

The transient simulations using COMSOL (finite element modelling), version 5.4, are performed on the reactor, considering only the active parts of the reactor: the three reaction media cylinders, the two TinT units and the reactor vessel just constrained to their heights. For computational simplicity, this reactor drawn in 3D as shown in Figure 2 (a) and (b), was then modelled in 2D for an axisymmetric cross-section shown in Figure 2 (c), by-default halved by COMSOL along the axis as in Figure 2 (d). In the present work, only desorption is modelled, where absorption is expected to be studies eventually. In Figure 2, the fluid inlets and outlets are indicated using arrows, where red represents the heat transfer fluid (HTF) and blue represents NH_3. Here only the NH_3 direction during desorption is shown, which originates within the reaction media and flows out of it as shown, from the top. For the absorption case, this NH_3 flow will be reversed, which will then flow into the reaction media from the bottom.

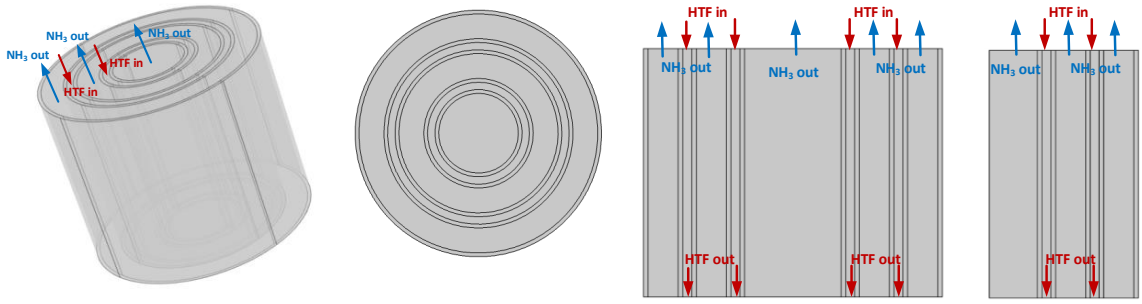

Figure 2. The reactor-HEX geometry modelled in COMSOL: (a) the 3D geometry in full, (b) from the top, (c) the 2D axisymmetric cross-section of this 3D geometry, and (d) a half (divided along the axis) of this 2D geometry.

The transient simulations are conducted through a stationary study for the HTF flow inside the HEXs and a time-dependent study on the reaction, heat transfer and gas flow phenomena. These are performed considering the desorption case, so far, for an HTF inlet temperature of 90 °C. The flow-field obtained from the stationary study (*spf.U*) is used as an input to the time-dependent study. The HTF considered is a silicon oil (Therm 180 (Lauda, 2019)) circulated in the HEXs using Lauda ECO Gold thermostat baths with an average volumetric flow rate of 0.183 l s^{-1} (a half of the maximum of 0.37 l s^{-1}). Therefore, the HTF flow regime is turbulent (with Reynolds numbers considerably above 2900) already at the inlets of each TinT units, with average and maximum velocities of 354 m s^{-1} and 709 m s^{-1} (TinT1, 517 mm^3 cross-section) and 192 m s^{-1} and 385 m s^{-1} (TinT2, 953 mm^3 cross-section). Thus, the stationary study is constructed using the *Turbulent flow module* (*k-ε* type) in COMSOL for the HTF flow within the HEX units.

In the time-dependent study, the involved physics (i.e., chemical kinetics and heat and mass transfer) of the reaction domains are solved in COMSOL, employing partial differential equations (PDEs), as shown in (eq. 2)-(eq. 7), using the respective physics modules: *heat transfer in porous media*, *domain ODEs and DAEs*, and *free and porous media flow*. In particular, these describe: heat transfer in all domains beside the salt bed (eq. 2), heat transfer in the porous salt-ammonia media (eq. 3), the chemical reaction rate (eq. 4), fluid flow in the salt-Al mesh porous media ((eq. 5) and (eq. 6)), and the fluid flow of the desorbed NH_3 gas (eq. 7). In (eq. 2), ρ is the density, c_p is the specific heat capacity at constant pressure, k is the thermal conductivity, T is the temperature and $\boldsymbol{u}$ is the flow field, equal to 0 in the solid domains. In (eq. 3) and (eq. 4), $\boldsymbol{da(t)/dt}$ is the reaction advancement rate, $\boldsymbol{N_s}$ is the number of stoichiometric amount of reacting NH_3 (mol/volume), $\boldsymbol{\Delta H}$ is the reaction enthalpy, $\boldsymbol{k_{0a}}$ and $\boldsymbol{k_{0d}}$ are the respective Arrhenius pre-exponential factors for absorption and desorption, $\boldsymbol{E_a}$ and $\boldsymbol{E_d}$ are the respective absorption and desorption activation energies, $\boldsymbol{a(t)}$ is the reaction advancement, $\boldsymbol{m_a}$ and $\boldsymbol{m_d}$ are the respective kinetic coefficients of absorption and desorption, $\boldsymbol{p_{eq}}$ is the equilibrium pressure, and $\boldsymbol{p}$ is the reactor pressure. In (eq. 5) and (eq. 6), $\boldsymbol{\varepsilon}$ is the porosity of the salt, $\boldsymbol{\rho}$ is NH_3 density, $\boldsymbol{Q_{br}}$ is the mass of source/sink, $\boldsymbol{MW_{NH3}}$ is NH_3 molecular weight, $\boldsymbol{\mu}$ is the dynamic viscosity of NH_3, $\boldsymbol{k_D}$ is the hydraulic permeability of salt, $\boldsymbol{\beta_F}$ is the Forcheimer drag factor, and $\boldsymbol{F}$ is the domain forces (neglected). In (eq. 7), $\boldsymbol{\rho}$ is NH_3 density, $\boldsymbol{\mu}$ is the dynamic viscosity of NH_3, $\boldsymbol{p}$ is the pressure, $\boldsymbol{u}$ is the velocity field, $\boldsymbol{F}$ is the forces that NH_3 gas is subject to (which are neglected). The hydraulic permeability of the salt $\boldsymbol{k_D}$ is calculated using the Carman-Kozeny equation as shown in (eq. 8), where the salt particles are assumed spherical with a diameter $\boldsymbol{d_p}$ of 0.5 mm.

$$\rho c_p \frac{\partial T}{\partial t} + \rho c_p \boldsymbol{u} \cdot \nabla T + \nabla(-k\nabla T) = 0 \qquad \text{(eq. 2)}$$

$$(\rho c_p)_{eff} \frac{\partial T}{\partial t} + \rho c_p \boldsymbol{u} \cdot \nabla T + \nabla\left(-k_{eff}\nabla T\right) \pm \frac{da(t)}{dt} N_s \cdot \Delta H_{des} = 0 \qquad \text{(eq. 3)}$$

$$\frac{da(t)}{dt} = k_{0a,d} exp\left(-\frac{E_{a,d}}{RT}\right)\left(1 - a(t)\right)^{m_{a,d}}\left(\frac{p_{eq} - p}{p_{eq}}\right) \qquad \text{(eq. 4)}$$

$$\frac{\partial \varepsilon \rho}{\partial t} + \nabla \cdot (\rho \boldsymbol{u}) = Q_{br}\,; \qquad Q_{br} = \pm \frac{da(t)}{dt} N_s \cdot MW_{NH3} \qquad \text{(eq. 5)}$$

$$\rho \frac{\partial \boldsymbol{u}}{\partial t} = \nabla \cdot \left[-p\boldsymbol{I} + \frac{\mu}{\varepsilon}(\nabla \boldsymbol{u} + (\nabla \boldsymbol{u})^T) - \frac{2}{3}\frac{\mu}{\varepsilon}(\nabla \cdot \boldsymbol{u})\boldsymbol{I}\right] - \left(\frac{\mu}{k_D} + \beta_F |\boldsymbol{u}| + \frac{Q_{br}}{\varepsilon^2}\right)\boldsymbol{u} + \boldsymbol{F} \qquad \text{(eq. 6)}$$

$$\rho \frac{\partial \boldsymbol{u}}{\partial t} + \rho(\boldsymbol{u} \cdot \boldsymbol{\nabla})\boldsymbol{u} = \nabla \cdot \left[-p\boldsymbol{I} + \mu(\nabla \boldsymbol{u} + (\nabla \boldsymbol{u})^T) - \tfrac{2}{3}\mu(\nabla \cdot \boldsymbol{u})\boldsymbol{I}\right] + \boldsymbol{F} \quad ; \quad \frac{\partial \boldsymbol{\rho}}{\partial \boldsymbol{t}} + \boldsymbol{\nabla} \cdot (\boldsymbol{\rho u}) = \boldsymbol{0} \qquad \text{(eq. 7)}$$

$$k_D = \frac{\varepsilon^3}{180(1-\varepsilon)^2} d_p^2 \quad \text{(eq. 8)}$$

A time step of 30 seconds and a total simulation time of 15 hours are used. These simulations, starting with coarse mesh sizing, were repeated for normal and fine mesh sizes, while obtaining consistent results. Therefore, fine mesh size is chosen as a representative enough mesh size. The porosity ε of the salt ($SrCl_2{\cdot}8NH_3$) alone is used as 0.28264 (for its true and bulk densities respectively of 1394 kg m^{-3} and 1000 kg m^{-3} (Soprani 2016, Lysgaard et al. 2012)). Whereas, the porosity ε of the $SrCl_2{\cdot}8NH_3$-EG composite is used as 0.30213 (for the density of graphite 2260 kg m^{-3} (Graphite, 2015) and the density of graphite in the EG board 75 kg m^{-3} (SGL CARBON GmbH, 2019)). The corresponding volume fractions of $SrCl_2{\cdot}8NH_3$ and EG in the composite (excluding the pore-volume) are thus 0.952 and 0.0476. The effective thermal conductivity of the composite was calculated as a volume average of the thermal conductivity of each material. Thermal conductivity of each salt was approximated to 1.1 W m^{-1} K^{-1} as per available data from literature (Jiang et al. 2013). The in-plane and through-plane thermal conductivities of graphite of the EG board were found to be respectively 26 W m^{-1} K^{-1} and 10.5 W m^{-1} K^{-1} by linear projection of the data from (SGL CARBON GmbH, 2019) for the compacted new density of EG: 172 kg m^{-3} (for 21 w/w% graphite in the composite with bulk density of 820 kg m^{-3}). The main simulation was performed considering the salt-EG composite. To analyze the influence of the EG in the heat transfer enhancement, a simulation trial was, in-addition, conducted for the case of salt-only, thus excluding EG (thus considering that the entire volume of 0.00210 m^3 to be filled with $SrCl_2{\cdot}8NH_3$ with a porosity ε of 0.30213). The property data of Al, SS and HTF Therm 180 were used from COMSOL standard materials library, assuming bulk solid Al, SS AISI 4340.1 and Silicon (liquid).

The initial temperature of the HTF fluid is set to 90 °C, while the initial temperature of the reaction media, HEX Al walls, and the SS reactor walls are also assumed to be at room temperature (25 °C). The initial pressure of the reactor is set to be 8 bar, and of the HEX is set to be 1 bar. The reaction advancement *a*, which is defined as zero for the condition where the salt is fully saturated with NH_3 (which should, upon complete desorption reach 1). The initial velocity field of NH_3 is assumed null (i.e, 0 m s^{-1}), while the flow rate of the HTF at the HEX inlet is considered to be 0.183 l s^{-1}. The velocity at the walls was considered null and the reactor casing to be adiabatic.

3 Results and discussion

The numerical simulation results obtained of the TCS reactor for desorption during 15 hours are discussed in this section. Indeed, a combined study of both desorption and absorption is important to draw general conclusions on reaction kinetics and, mass and heat transfer, and therefore absorption analysis will be a key future step. In the present desorption modelling, the stationary study yielded the velocity profile of the HTF inside the two HEX units, as detailed in section 2.1. By employing the resultant HTF velocity profile into the time-dependent study, the reaction progression behavior within this TinT HEXs-based reactor configuration is analyzed within the considered 15 hours of reaction time, along the temperature evolution, velocity of NH_3 evolution and reaction advancement in sections 2.2-2.4. These results are shown for several chosen time steps as examples at 0 s, 900 s, 1800 s, 3600 s (1 h), 10800 s (3 h), 18000 s (5 h), 36000 s (10 h) and 54000 s (15 h).

2.1. Heat exchanger velocity profile

The velocity profiles of the HTF (in the turbulent regime) within the two TinT HEXs found through the stationary study are shown in Figure 3; in (a) on the chosen 2D cross-section and in (b) on a projection of this cross-section into two thirds of the 3D reactor. The flow direction is identified with black and red arrows, respectively in the 2D and the 3D profiles. The velocity of the HTF lies within a range of 0.17-0.27 m s^{-1}, as results indicate. The specific turbulent flow profile from this stationary study *spf.U* as in Figure 3 is fed into the consecutive time-dependent study of the reaction.

2.2. Reactor temperature profiles

The temperature evolution inside the considered part of the reactor during desorption is shown at the chosen example time-steps in-terms of isothermal contours in the 2D cross-section as in Figure 4, and in-terms of temperature regions in the 3D projection as in Figure 5. By the end of the total 15 hours of reaction time, the considered reactor+HEX unit has reached temperatures of 88.80-89.97 °C, implying that the system has reached nearly isothermal conditions (for the employed HTF inlet temperature of 90 °C). As seen, the temperature inside the reactor evolves faster and closer to the HEX walls, and more so at the HTF inlets. With time, the temperature profile in the reactor becomes somewhat asymmetric, evolving into increasingly higher temperature regions at the outer reaction media cylinders

as compared to the innermost reaction media cylinder. This can be reasoned with the larger thickness (i.e., the distance heat transfer needs to occur) of the innermost reaction media cylinder and which therefore has higher thermal mass as compared to the outer reaction cylinders.

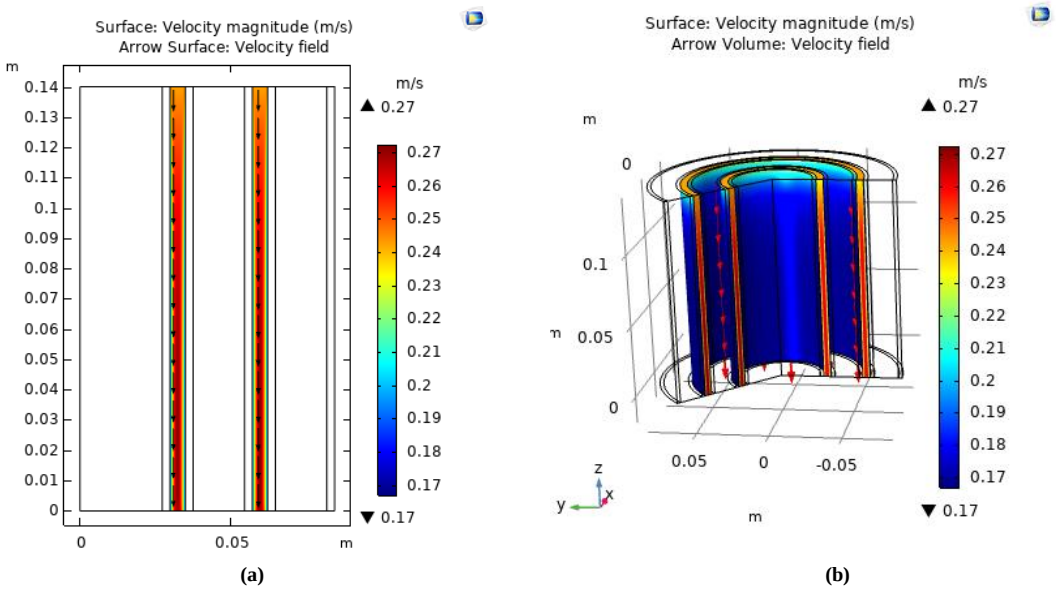

(a) **(b)**

Figure 3. The velocity profiles of the HTF (a) in 2 D (b) in 3D (the arrows indicate the flow direction)

2.3. Reactor – NH_3 flow during desorption

NH_3 flow velocity inside the reactor during desorption propagation can be seen in Figure 6, with the flow direction identified with red arrows located where NH_3 leaves the reaction media. The flow velocity of NH_3 varies in each reaction media region, however, as can be seen, lies within a range of 0 m s^{-1} to a maximum of 1.85×10^{-3} m s^{-1} during the considered reaction period of 15 hours. The 0 m s^{-1} occurs at initial conditions as well as in the regions that have completely desorbed with time. As also can be seen, the velocity evolution is also dominating at the HTF inlet side (top of the reactor), while the two outer-cylinders of reaction media undergo more desorption as compared to the innermost reaction media. These results imply that e.g. an additional HEX tube that could run along the center axis of the reactor could significantly improve the reaction rate, particularly within the innermost reaction media cylinder.

2.4. Reaction advancement

The reaction advancement (a) is shown along the employed 15 hour time-period in a 3D projection of the reactor in Figure 7. Analogous to the temperature and NH_3 velocity evolution within the reactor, the reaction (desorption in this study) advancement also occurs more at outer reaction cylinders, with somewhat lesser within the innermost reaction media cylinder. These results also therefore confirm the significance of an additional HEX component along e.g. the center-axis of the reactor. The reaction advancement has reached 0.85 or above in the entirety of reaction media during these 15 hours. For 100% desorption (i.e., to reach a=1 in the entirety of reaction media), longer time will be required, as reaction will slow-down with further advancement. This is however excluded herein, as the main purpose of the study is to analyze the effects of the HEX geometry and the EG in improving reaction kinetics.

The simulations conducted for the case of using salt-alone (i.e., no EG) yielded a reaction advancement of only 0.55 and above at the end of the total 15 hours' reaction time, which is therefore slightly lower than the case with EG. These final reaction advancements are compared in Figure 8, respectively for the composite with EG (a) and without EG (i.e., purely salt) (b). Indeed, even if combining the salt with EG enhances heat transfer, it the same time creates compromises in either the available storage capacity of the TCS or the mass transfer rate as either the amount of salt or the porosity decreases for a given reactor volume. With this type of numerical simulations as in this work, finding the best compromise between heat and mass transfer can be effectively identified.

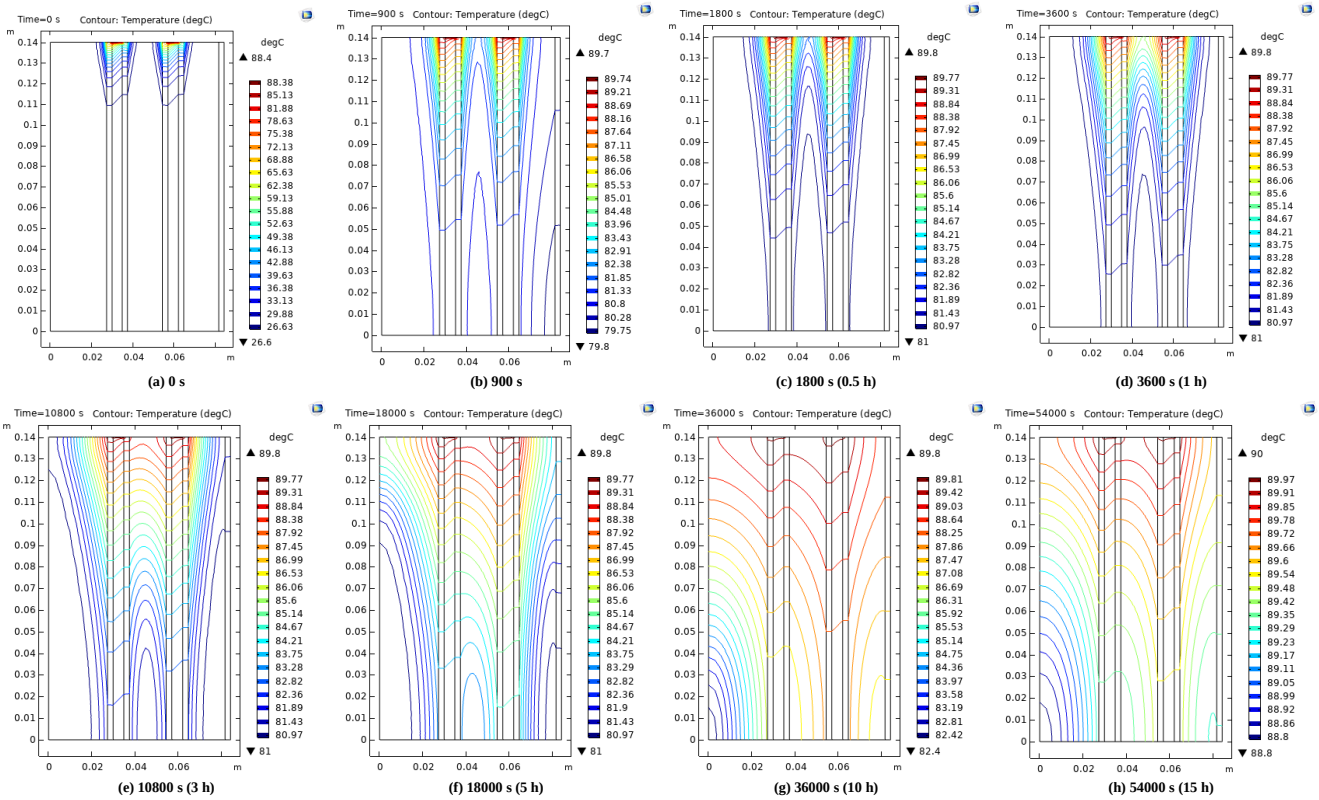

(a) 0 s **(b) 900 s** **(c) 1800 s (0.5 h)** **(d) 3600 s (1 h)**

(e) 10800 s (3 h) **(f) 18000 s (5 h)** **(g) 36000 s (10 h)** **(h) 54000 s (15 h)**

Figure 4. The temperature evolution in the reactor during desorption in-terms of isothermal contours from 0-54000 s (15 hours), in (a)-(h)

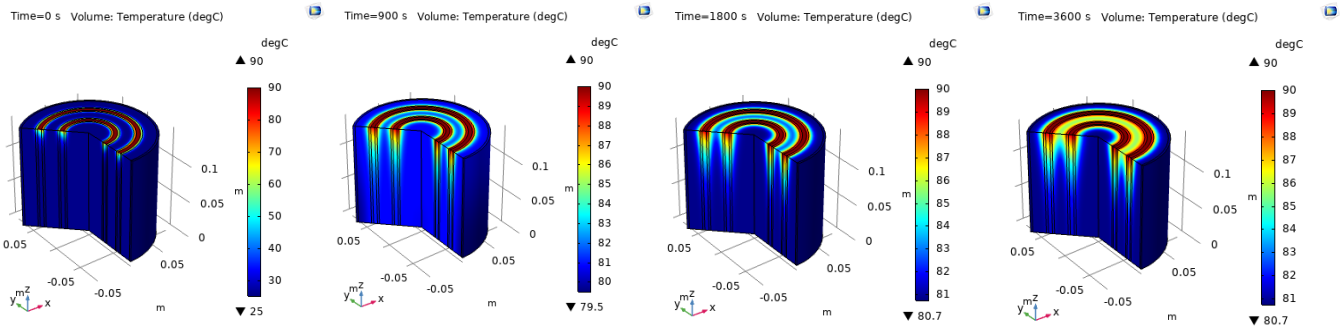

(a) 0 s **(b) 900 s** **(c) 1800 s (0.5 h)** **(d) 3600 s (1 h)**

(e) 10800 s (3 h) **(f) 18000 s (5 h)** **(g) 36000 s (10 h)** **(h) 54000 s (15 h)**

Figure 5. The temperature evolution in the reactor during desorption in-terms of temperature regions projected in 3D, from 0--54000 s (15 hours), in (a)-(h)

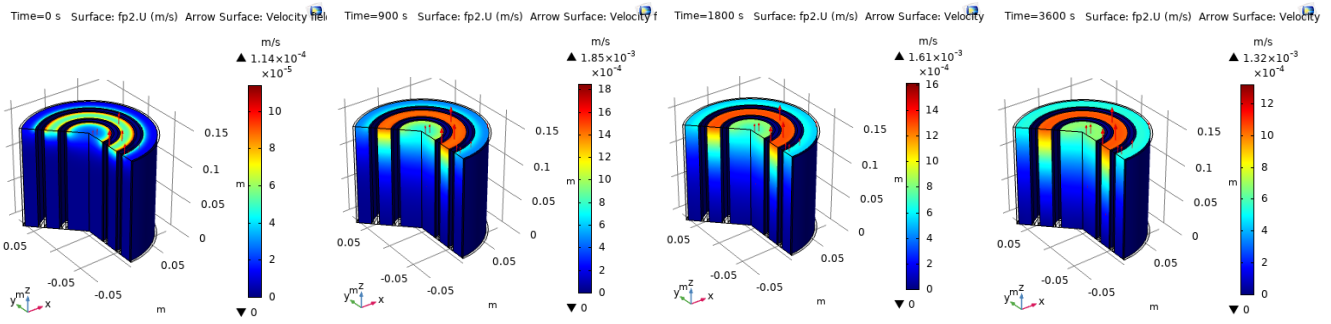

(a) 0 s **(b) 900 s** **(c) 1800 s (0.5 h)** **(d) 3600 s (1 h)**

(e) 10800 s (3 h) **(f) 18000 s (5 h)** **(g) 36000 s (10 h)** **(h) 54000 s (15 h)**

Figure 6. The velocity evolution of NH_3 produced during desorption in the reactor projected in 3D, from 0--54000 s (15 hours), in (a)-(h)

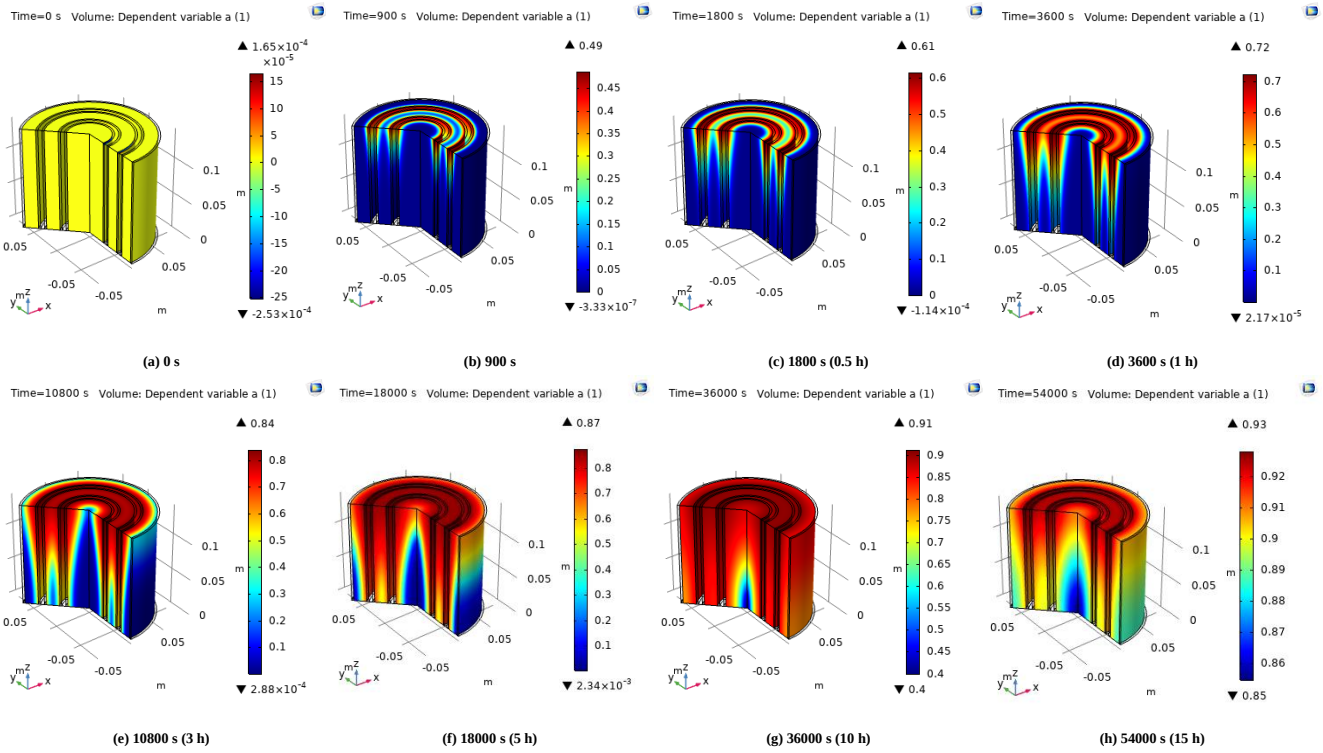

(a) 0 s **(b) 900 s** **(c) 1800 s (0.5 h)** **(d) 3600 s (1 h)**

(e) 10800 s (3 h) **(f) 18000 s (5 h)** **(g) 36000 s (10 h)** **(h) 54000 s (15 h)**

Figure 7. The reaction advancement in desorption projected in 3D, from 0--54000 s (15 hours), in (a)-(h

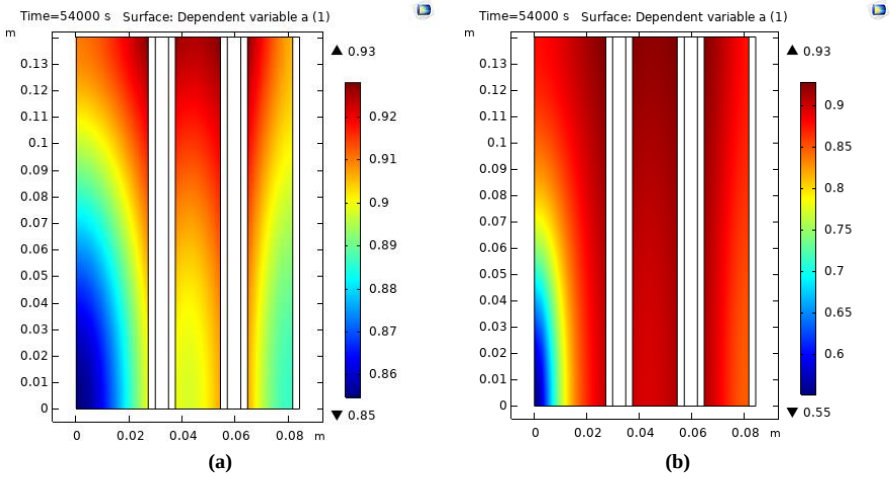

Figure 8. The reaction advancements at the end of total 15 hours, for (a) with EG and (b) without EG

4 Concluding remarks

Numerical modeling of a reactor-heat exchanger combined unit of a TCS system in COMSOL in 2D, for the reversible chemical reaction between $SrCl_2 \cdot NH_3$ and $SrCl_2 \cdot 8NH_3$ is conducted with the aim of finding an optimal configuration of a reactor-HEX unit. The 2 l (effective volume) packed-bed reactor is designed to store 0.5 kWh of heat above ~81 ℃ at or below 8 bar during desorption. The transient simulations in COMSOL results describe the heat and mass transfer, reaction kinetics and fluid flow phenomena for this reactor employing a composite of $SrCl_2 \cdot 8NH_3$ and EG (with volume fractions 0.665 and 0.0332) combined with two TinT HEX sections to provide the required heat of desorption. The employed volume fraction of graphite manages to improve the reaction advancement significantly. For instance, for a total of 15 hours reaction time, the reaction advancement for the salt-EG composite reaches above 0.85 whereas when the salt-alone was used (i.e., excluding EG) this is only above 0.55. The two TinT units contribute to reasonable heat transfer within the reactor, while, the results imply that if an additional unit of HEX is installed along the center-axis of the reactor, the reaction time can be further reduced. This work exemplifies the effectiveness of this new and simple HEX-configuration in improving the reaction kinetics, accommodating better heat exchange between the HTF and reaction media, as compared to the current state-of-the-art of HEXs for NH_3-metal halide reaction-based TCS systems. As future work, the effects of effects of effective HEX thickness and number of TinT units (including one along the center-axis of the reactor), reversing the HTF flow direction, as well as the other chosen reactor+HEX configurations will be analyzed through similar numerical simulations. Thereby, the optimal reactor-HEX configuration will be chosen to construct in a bench-scale TCS system at KTH. This is expected to work as a test-bed for the TCS technology using this chemical reaction system, for different operating conditions including solar-thermal heat storage.

5 Acknowledgments

The authors acknowledge Nordforsk for funding this research project: Neutrons for Heat Storage (NHS).

6 References

Al-Zareer, M., Dincer, I., & Rosen, M. A. (2017). Heat Transfer and Thermodynamic Analyses of a Novel Solid-Gas Thermochemical Strontium Chloride-Ammonia Thermal Energy Storage System. *Journal of Heat Transfer*, *140*(February), 1–17. https://doi.org/10.1115/1.4037534

Bao, H. S., Wang, R. Z., Oliveira, R. G., & Li, T. X. (2012). Resorption system for cold storage and long-distance refrigeration. *Applied Energy*, *93*, 479–487. https://doi.org/10.1016/j.apenergy.2011.12.022

Barzin, R., Chen, J. J. J., Young, B. R., & Farid, M. M. (2015). Peak load shifting with energy storage and price-based control system. *Energy*, *92*, 505–514. https://doi.org/10.1016/j.energy.2015.05.144

Chiu, J. N. W., Castro Flores, J., Martin, V., & Lacarrière, B. (2016). Industrial surplus heat transportation for use in district heating. *Energy*, *110*, 139–147. https://doi.org/10.1016/j.energy.2016.05.003

COMSOL Inc. (2019). COMSOL-Multiphysics simulation just got better, faster, more accessible. Retrieved March 21, 2019, from https://www.comsol.se/

Damstahl. (1998). *Driftstryck för rostfria rör*. Retrieved from https://www.damstahl.se/globalassets/downloads-130x185/sverige/downloads/driftstryck-for-rostfria-ror..pdf

Erhard, A., Spindler, K., & Hahne, E. (1998). Test and simulation of a solar powered solid sorption cooling machine. *International Journal of Refrigeration*, *21*(2), 133–141. https://doi.org/10.1016/S0140-7007(97)00065-0

Frazzica, A., & Freni, A. (2017). Adsorbent working pairs for solar thermal energy storage in buildings. *Renewable Energy*, *110*, 87–94. https://doi.org/10.1016/j.renene.2016.09.047

Fujii, S., Horie, N., Nakaibayashi, K., Kanematsu, Y., Kikuchi, Y., & Nakagaki, T. (2019). Design of zeolite boiler in thermochemical energy storage and transport system utilizing unused heat from sugar mill. *Applied Energy*, *238*, 561–571. https://doi.org/10.1016/j.apenergy.2019.01.104

Graphite, P. (2015). Properties and Characteristics. In *Properties and Characteristics of Graphite- For industrial applications*. Retrieved from http://poco.com/Portals/0/Literature/Semiconductor/IND-109441-0115.pdf

Jiang, L., Wang, L. W., Jin, Z. Q., Wang, R. Z., & Dai, Y. J. (2013). Effective thermal conductivity and permeability of compact compound ammoniated salts in the adsorption/desorption process. *International Journal of Thermal Sciences*. https://doi.org/10.1016/j.ijthermalsci.2013.03.017

Jiang, L., Wang, L. W., Liu, C. Z., & Wang, R. Z. (2016). Experimental study on a resorption system for power and refrigeration cogeneration. *Energy*, *97*, 182–190. https://doi.org/10.1016/j.energy.2015.12.128

Kuwata, K., Masuda, S., Kobayashi, N., Fuse, T., & Okamura, T. (2016). Thermochemical Heat Storage Performance in the Gas/Liquid-Solid Reactions of SrCl2 with NH3. *Natural Resources*, *07*(11), 655–665. https://doi.org/10.4236/nr.2016.711052

Lauda. (2019). *LAUDA Heat transfer liquids - Thermostats, Circulation chillers, Water baths*. Lauda-Koenigshofen.

Li, T. X., Wang, R. Z., Kiplagat, J. K., & Chen, H. (2010). Experimental study and comparison of thermochemical resorption refrigeration cycle and adsorption refrigeration cycle. *Chemical Engineering Science*, *65*(14), 4222–4230. https://doi.org/10.1016/j.ces.2010.04.022

Li, T. X., Wang, R. Z., Wang, L. W., & Kiplagat, J. K. (2009). Study on the heat transfer and sorption characteristics of a consolidated composite sorbent for solar-powered thermochemical cooling systems. *Solar Energy*, *83*(9), 1742–1755. https://doi.org/10.1016/j.solener.2009.06.013

Li, T. X., Wang, R. Z., & Yan, T. (2015). Solid-gas thermochemical sorption thermal battery for solar cooling and heating energy storage and heat transformer. *Energy*, *84*, 745–758. https://doi.org/10.1016/j.energy.2015.03.040

Li, T. X., Xu, J. X., Yan, T., & Wang, R. Z. (2016). Development of sorption thermal battery for low-grade waste heat recovery and combined cold and heat energy storage. *Energy*, *107*, 347–359. https://doi.org/10.1016/j.energy.2016.03.126

Lysgaard, S., Ammitzbøll, A. L., Johnsen, R. E., Norby, P., Quaade, U. J., & Vegge, T. (2012). Resolving the stability and structure of strontium chloride amines from equilibrium pressures, XRD and DFT. *International Journal of Hydrogen Energy*, *37*(24), 18927–18936. https://doi.org/10.1016/j.ijhydene.2012.09.129

Mofidi, S. A. H., & Udell, K. S. (2017). Study of Heat and Mass Transfer in MgCl2/NH3 Thermochemical Batteries. *Journal of Energy Resources Technology*, *139*(3), 032005. https://doi.org/10.1115/1.4035750

NagaMalleswara Rao, K., Ram Gopal, M., & Bhattacharyya, S. (2013). Analysis of a SrCl 2 –NH 3 solid sorption refrigeration system . *International Journal of Low-Carbon Technologies*, *10*(4), 365–373. https://doi.org/10.1093/ijlct/ctt046

SGL CARBON GmbH. (2019). *SIGRATHERM L and LN - Graphite lightweight board for thermal management*. Retrieved from SGL CARBON Gmb

Soprani, S. (2016). *MODELING – TES system based on SrCl 2 - NH 3*. Roskilde.

Swagelok. (2019). 304 / 304L and 316 / 316L Seamless , Instrumentation Grade Tubing. Retrieved from Product Specification PDF website: https://www.swagelok.com/en/catalog/Product/Detail?part=SS-T6M-S-1.0M-6ME

Valverde, J. M., Barea-López, M., Perejón, A., Sánchez-Jiménez, P. E., & Pérez-Maqueda, L. A. (2017). Effect of Thermal Pretreatment and Nanosilica Addition on Limestone Performance at Calcium-Looping Conditions for Thermochemical Energy Storage of Concentrated Solar Power. *Energy and Fuels*, *31*(4), 4226–4236. https://doi.org/10.1021/acs.energyfuels.6b03364